Cancer predisposition and hematopoietic failure in *Rad50*$^{S/S}$ mice

Carla F. Bender,[1] Michael L. Sikes,[2] Ruth Sullivan,[3] Leslie Erskine Huye,[4] Michelle M. Le Beau,[6] David B. Roth,[4,5] Olga K. Mirzoeva,[1] Eugene M. Oltz,[2] and John H. J. Petrini[1,7,8]

[1]Laboratory of Genetics, University of Wisconsin Medical School, Madison, Wisconsin 53706 USA; [2]Department of Microbiology & Immunology, Vanderbilt University School of Medicine, Nashville, Tennessee 37232, USA; [3]Waisman Center and Department of Pathobiological Sciences, School of Veterinary Medicine, University of Wisconsin-Madison, Madison, Wisconsin 53705, USA; [4]Department of Immunology and [5]Howard Hughes Medical Institute, Baylor College of Medicine, Houston, Texas 77030, USA; [6]Section of Hematology/Oncology, Department of Medicine, University of Chicago, Chicago, Illinois 60637, USA; [7]Molecular Biology Program, Memorial Sloan Kettering Cancer Center and Cornell University Graduate School of Medical Sciences, New York, New York 10021, USA

Mre11, Rad50, and Nbs1 function in a protein complex that is central to the metabolism of chromosome breaks. Null mutants of each are inviable. We demonstrate here that hypomorphic *Rad50* mutant mice (*Rad50*$^{S/S}$ mice) exhibited growth defects and cancer predisposition. *Rad50*$^{S/S}$ mice died with complete bone marrow depletion as a result of progressive hematopoietic stem cell failure. Similar attrition occurred in spermatogenic cells. In both contexts, attrition was substantially mitigated by p53 deficiency, whereas the tumor latency of *p53*$^{-/-}$ and *p53*$^{+/-}$ animals was reduced by *Rad50*$^{S/S}$. Indices of genotoxic stress and chromosomal rearrangements were evident in *Rad50*$^{S/S}$ cultured cells, as well as in *Rad50*$^{S/S}$ and *p53*$^{-/-}$ *Rad50*$^{S/S}$ lymphomas, suggesting that the *Rad50*$^{S/S}$ phenotype was attributable to chromosomal instability. These outcomes were not associated with overt defects in the Mre11 complex's previously established double strand break repair and cell cycle checkpoint regulation functions. The data indicate that even subtle perturbation of Mre11 complex functions results in severe genotoxic stress, and that the complex is critically important for homeostasis of proliferative tissues.

[*Key Words:* Mre11 complex; Rad50S; double strand breaks; hematopoiesis]

Received May 14, 2002; revised version accepted July 3, 2002.

The Mre11 complex, consisting of the highly conserved Mre11 and Rad50 proteins and Nbs1 (or Xrs2 in yeast), mediates diverse functions in double strand break (DSB) metabolism. In both mammals and *Saccharomyces cerevisiae*, the complex functions as a sensor of DSBs and influences the induction of DNA damage-dependent cell cycle checkpoints (Petrini 2000a; D'Amours and Jackson 2001; Grenon et al. 2001; Mirzoeva and Petrini 2001; Usui et al. 2001). Mre11 complex deficiency in *S. cerevisiae* profoundly impairs recombinational DNA repair as well as telomere maintenance and meiotic recombination (Haber 1998). In vertebrates, null mutants in each member of the Mre11 complex are inviable (Xiao and Weaver 1997; Luo et al. 1999; Yamaguchi-Iwai et al. 1999; Zhu et al. 2001).

The Mre11 complex specifies ssDNA endonuclease, 3′-to-5′ exonuclease, and DNA unwinding activities in vitro. Accordingly, it has been implicated in DNA end processing events in vivo. Spo11, the topoisomerase II-like enzyme that forms DSBs to initiate meiotic recombination, remains bound to the DSB termini in a group of hypomorphic *RAD50* and *MRE11* mutants, called *S* mutants (Alani et al. 1990; Usui et al. 1998). This suggests that the Spo11-DNA intermediate is cleaved by the Mre11 complex in wild-type cells.

In addition, *rad50S* and nuclease-deficient *mre11* mutants are inviable in the absence of Rad27, a nuclease required for the completion of lagging strand DNA synthesis, raising the possibility that the Mre11 complex participates in the nucleolytic processing of DNA replication intermediates (Harrington and Lieber 1994; Moreau et al. 1999; Debrauwere et al. 2001). It appears that Mre11 complex nuclease activities are not critical to its DSB repair functions because *rad50S*, *mre11S*, and nuclease-deficient *mre11* mutants exhibit only minor sensitivity to clastogens, and resection of DSBs generated by the HO endonuclease is normal (Alani et al. 1990; Nairz and Klein 1997; Bressan et al. 1998, 1999; Tsubouchi and Ogawa 1998; Usui et al. 1998; Moreau et al. 1999; Lee et al. 2002).

As suggested by the functional interaction with Rad27, the Mre11 complex appears to be particularly important during DNA replication (Petrini 2000b). γ-irradiation of synchronous cultures revealed that the ex-

[8]Corresponding author.
E-MAIL petrinij@mskcc.org; FAX (646) 422-2062.
Article and publication are at http://www.genesdev.org/cgi/doi/10.1101/gad.1007902.

treme clastogen sensitivity of *S. cerevisiae mre11*Δ mutants is largely attributable to the inability of those cells to utilize sister chromatids in DNA repair, and that this effect is most pronounced in S phase (Ivanov et al. 1992; Bressan et al. 1999). Further, SbcCD, the bacterial Mre11 complex ortholog, appears to be required for processing aberrant DNA structures that arise at replication forks (Leach 1994; Connelly et al. 1998). In bacteriophage T4, recombination-dependent DNA replication and restart of stalled replication forks requires gp46/47, the T4 orthologs of Mre11/Rad50 (George et al. 2001; Stohr and Kreuzer 2001).

Several lines of evidence support a similar role for the Mre11 complex in vertebrates. First, Mre11-depleted DT40 chicken cells die with chromosomal damage suggestive of failure to resolve DSBs arising during DNA replication (Yamaguchi-Iwai et al. 1999). Second, DNA replication in Mre11-depleted *Xenopus laevis* extracts is associated with the accumulation of chromosome breaks (Costanzo et al. 2001). Finally, the human Mre11 complex becomes avidly associated with chromatin during S phase (Maser et al. 2001). These studies underscore the role of the Mre11 complex in DNA replication, and define a likely basis for the inviability of Mre11 complex-deficient vertebrate cells.

Mre11 complex functions at telomeres may also account for the inviability of Mre11 complex-deficient mammalian cells. The complex functions at telomeres in *S. cerevisiae* as well as in mammals, although the extent to which Mre11 complex telomere functions are conserved in yeast and mammalian cells is unknown. The human Mre11 complex is situated at telomeres via physical association with the telomere protection protein, TRF2 (Zhu et al. 2000). Given its association with TRF2, the Mre11 complex may function in telomere protection, and would be required for cellular viability via a role in preventing telomere failure (de Lange and Petrini 2000; Lombard and Guarente 2000; Zhu et al. 2000).

In this study, mice harboring a *Rad50* allele analogous to the *S. cerevisiae rad50S* allele *rad50-R20M* (Alani et al. 1990) were derived. $Rad50^{S/S}$ mice were viable, but exhibited partial embryonic lethality, growth defects, and cancer predisposition. These pathologic outcomes were associated with progressive failure of $Rad50^{S/S}$ hematopoietic and germline cells which was partially mitigated by p53 deficiency. Primary and transformed cell cultures and tumor lines established from $Rad50^{S/S}$ mice were characterized by increased spontaneous apoptosis and chromosomal instability. We conclude that this effect of the $Rad50^{K22M}$ allele constitutes the mechanistic basis of hematopoietic and spermatogenic depletion in $Rad50^{S/S}$ mice. These findings underscore the importance of the Mre11 complex for maintenance of chromosome stability and in homeostasis of proliferative tissues.

Results

Derivation of $Rad50^{S/S}$ *mice*

Null *Rad50* mutations were lethal at the cellular and organismal levels, precluding conventional gene inactivation as a means to analyze the Mre11 complex in vivo (Luo et al. 1999). Three hypomorphic *Rad50* mutants, $Rad50^{K6E}$, $Rad50^{K22M}$, and $Rad50^{R83I}$, corresponding to *S. cerevisiae rad50S* alleles were tested for their ability to support cell viability. $mRad50^{Brdm1}/mRad50^{Brdc1}$ embryonic stem (ES) cells harbor a null *Rad50* allele ($mRad50^{Brdm1}$) and a *Rad50* allele that is inactivated upon expression of *Cre* recombinase ($mRad50^{Brdc1}$). Because Rad50 is required for viability, *Cre* expression in $mRad50^{Brdm1}/mRad50^{Brdc1}$ cells is lethal unless a functional *Rad50* cDNA is ectopically expressed (Luo et al. 1999). These cells were cotransfected with a *Cre* expression vector (*pPGKhygro-Cre*) and a wild-type or *Rad50S* cDNA expression construct. Wild-type and $pRad50^{K22M}$, but not $pRad50^{R83I}$ or $pRad50^{K6E}$, were sufficient for viability. On this basis, the $Rad50^{K22M}$ mutation, which corresponds to the *rad50S* allele *rad50-R20M* in yeast (Alani et al. 1990), was chosen for the derivation of mutant mice.

pkin-24ploxp contains exons 1, 2, and 3 of the *Rad50* locus with an AAG to ATG change in exon 1, resulting in K→M at amino acid residue 22 (Fig. 1A; Dolganov et al. 1996). Homologous integration of *pkin-24ploxp* in ES cells was assessed by Southern blotting (Fig. 1B), and the ensuing targeted ES cells were used to derive mutant animals. $Rad50^{S/S}$ mice were susceptible to partial embryonic lethality at embryonic day 14–16 (E14–E16; $P = 0.002$), and were significantly underrepresented among 3-wk-old animals ($P = 0.00001$). These data indicated that the $Rad50^{K22M}$allele is hypomorphic.

$Rad50^{S/S}$ MEFs were not sensitive to ionizing radiation (IR), mitomycin C, hydroxyurea, or etoposide, nor did they exhibit growth defects. The formation of Mre11 IR-induced foci (IRIF) and the intra-S phase checkpoint were also unaffected (data not shown). In addition, wild-type levels of Mre11, Nbs1, and $Rad50S^{K22M}$ protein were present in extracts of $Rad50^{S/S}$ murine embryonic fibroblasts (MEFs), and their ability to assemble in complex was not overtly affected (Fig. 1C).

Although the $Rad50^{K22M}$ allele exerted a minimal cellular phenotype, it had a profound impact at the organismal level. $Rad50^{S/S}$ mice weighed 60% of wild-type littermates, and by 4–8 wk of age, most $Rad50^{S/S}$ animals had a gray, wasted appearance suggestive of anemia. The mean age of death of $Rad50^{S/S}$ mice was 2.6 ± 1.8 mo (N = 166). Whereas most $Rad50^{S/S}$ mice died tumor-free by 4 mo of age, 20% survived 4–7 mo. In this group of long-lived $Rad50^{S/S}$ mice, 20% died with metastatic thymic lymphomas, four exhibited splenic hyperplasia, and one mouse developed myeloid leukemia.

Meiotic progression in $Rad50^{S/S}$ *mice*

In *S. cerevisiae rad50S* mutants, meiotic DSBs are not processed due to the covalent attachment of Spo11 (Alani et al. 1990; Keeney and Kleckner 1995; Keeney et al. 1997). Because the function of Spo11 appears to be conserved in mice (Baudat et al. 2000; Romanienko and Camerini-Otero 2000), we analyzed $Rad50^{S/S}$ ovaries and

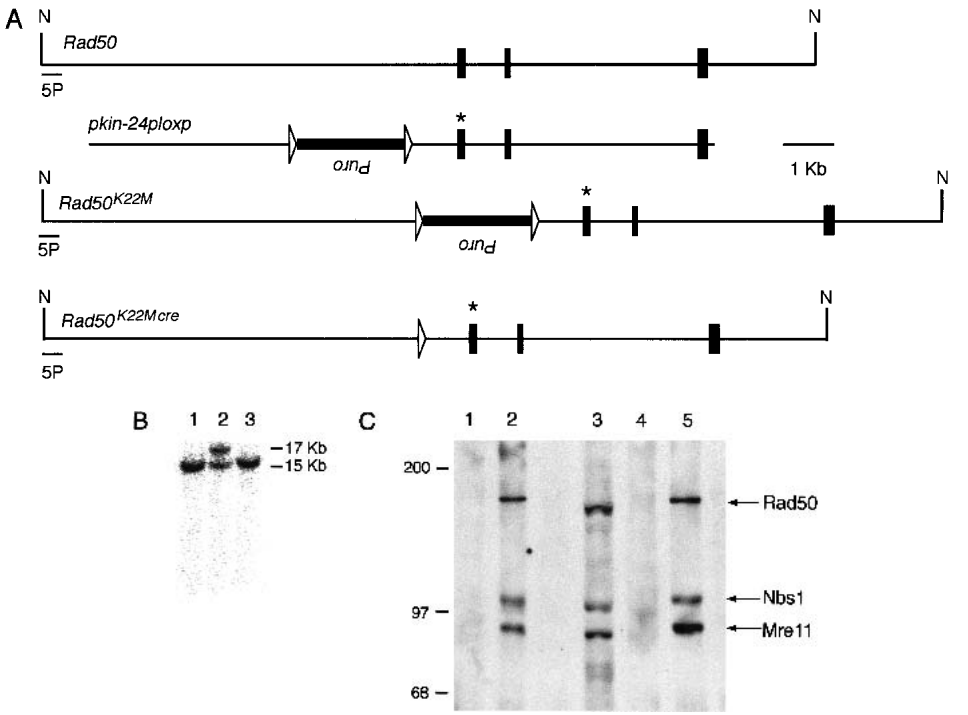

Figure 1. Derivation of *Rad50*^{K22M} mutants. (*A*) Schematic of *Rad50* locus. 5′ region and exons 1–3 (black boxes) are shown. Homologous integration of the targeting vector *pk-in-24ploxp* with the K22M mutation encoded in exon 1 (*) inserts a *loxP*-flanked (triangles) *puromyocin-resistance* gene (*Puro*) antisense and 5′ of *Rad50* and creates the *Rad50*^{K22M} allele. Cre-mediated deletion of *Puro* creates the *Rad50*^{K22Mcre} allele. N, *Nco*I; 5P, 5′ probe. (*B*) Southern blot analysis of *Nco*I-digested DNA hybridized with the 5′ probe shown in *A*. The *Rad50* and *Rad50*^{K22M} alleles yield 15 and 17 Kb fragments, respectively. (Lane *2*) Targeted ES cell clone. (Lanes *1*,*3*) Untargeted clones. (*C*) *Rad50*$^{+/+}$ (lanes *1*,*2*) or *Rad50*$^{S/S}$ (lanes *4*,*5*) immunoprecipitations performed with preimmune (lanes *1*,*4*) or Nbs1 antisera (lanes *2*,*5*). Whole-cell extract of *Rad50*$^{S/S}$ MEFs (lane *3*) included as control. Samples were immunoblotted sequentially with Nbs1, Mre11, and Rad50 antisera. Size markers (KD) are shown.

testes to determine whether murine *Rad50*^{K22M} led to an analogous block in meiotic progression.

Rad50$^{S/S}$ females were fertile and had normal ovaries (not shown). Testicular development was normal in prepubescent *Rad50*$^{S/S}$ males. Despite decreased cellularity in the seminiferous tubules of 4-wk-old *Rad50*$^{S/S}$ mice (Fig. 2A), older mice were also fertile.

Meiotic recombination defects in *Spo11*$^{-/-}$ mice result in depletion of germ cell precursors (Baudat et al. 2000; Romanienko and Camerini-Otero 2000). We reasoned that the cellular attrition in *Rad50*$^{S/S}$ testes might be the result of a similar, though less severe meiotic defect. TUNEL analysis of 4-wk-old *Rad50*$^{S/S}$ testes, unlike those from 2-wk-old *Rad50*$^{S/S}$ mice, revealed a 3–5-fold increase in the number of apoptotic tubules (Fig. 2B). However, cytologic analysis of meiotic progression did not indicate a stage-specific arrest, nor were aberrant chromosomal structures noted (Fig. 2C). These data suggest that the *Rad50*^{K22M} allele did not impair meiotic recombination, and that cell death in *Rad50*$^{S/S}$ testes is attributable to a different source of genotoxic stress.

Hematopoietic stem cell failure in Rad50$^{S/S}$ *mice*

The premature death of *Rad50*$^{S/S}$ mice was associated with severe anemia. Two-wk-old *Rad50*$^{S/S}$ mice did not exhibit differences in the abundance of hematopoietic cells. However, by 4–8 wk of age, the bone marrow of most *Rad50*$^{S/S}$ mice was virtually devoid of hematopoietic cells and was largely composed of adipocytes (Fig. 3A). Spleen and thymus architecture was also grossly abnormal, with few lymphocytes present (data not shown). Long-lived *Rad50*$^{S/S}$ mice that did not develop thymic lymphomas died with bone marrow attrition identical to that seen in 4–8-wk-old mutants.

Fluorescence-activated cell sorting (FACS) analysis was used to correlate abundance of hematopoietic components with age. Double negative ($CD4^-$,$CD8^-$, DN) T cells, pro B cells ($B220^+$,$CD43^+$), and macrophages ($B220^-$,$CD43^+$) were present at wild-type levels in E16 *Rad50*$^{S/S}$ embryos (Fig. 3B). By 1 wk of age, pre B ($B220^+$,$CD43^-$) and immature B ($B220^+$,IgM^+) cells in *Rad50*$^{S/S}$ mice were 1.5–3-fold reduced, whereas pro B cells and macrophages were 2–3-fold increased. Thymocytes were unaffected at this age, but splenic B and T cells were decreased to 4.8%–12% and 7%–49% of wild-type, respectively (Fig. 3B; data not shown). By 4 wk of age, lymphocytes, macrophages, red blood cells and platelets were severely depleted (0.1%–18% wild-type, Fig. 3B, data not shown). These results demonstrated that progressive hematopoietic failure in *Rad50*$^{S/S}$ mice affected all hematopoietic lineages.

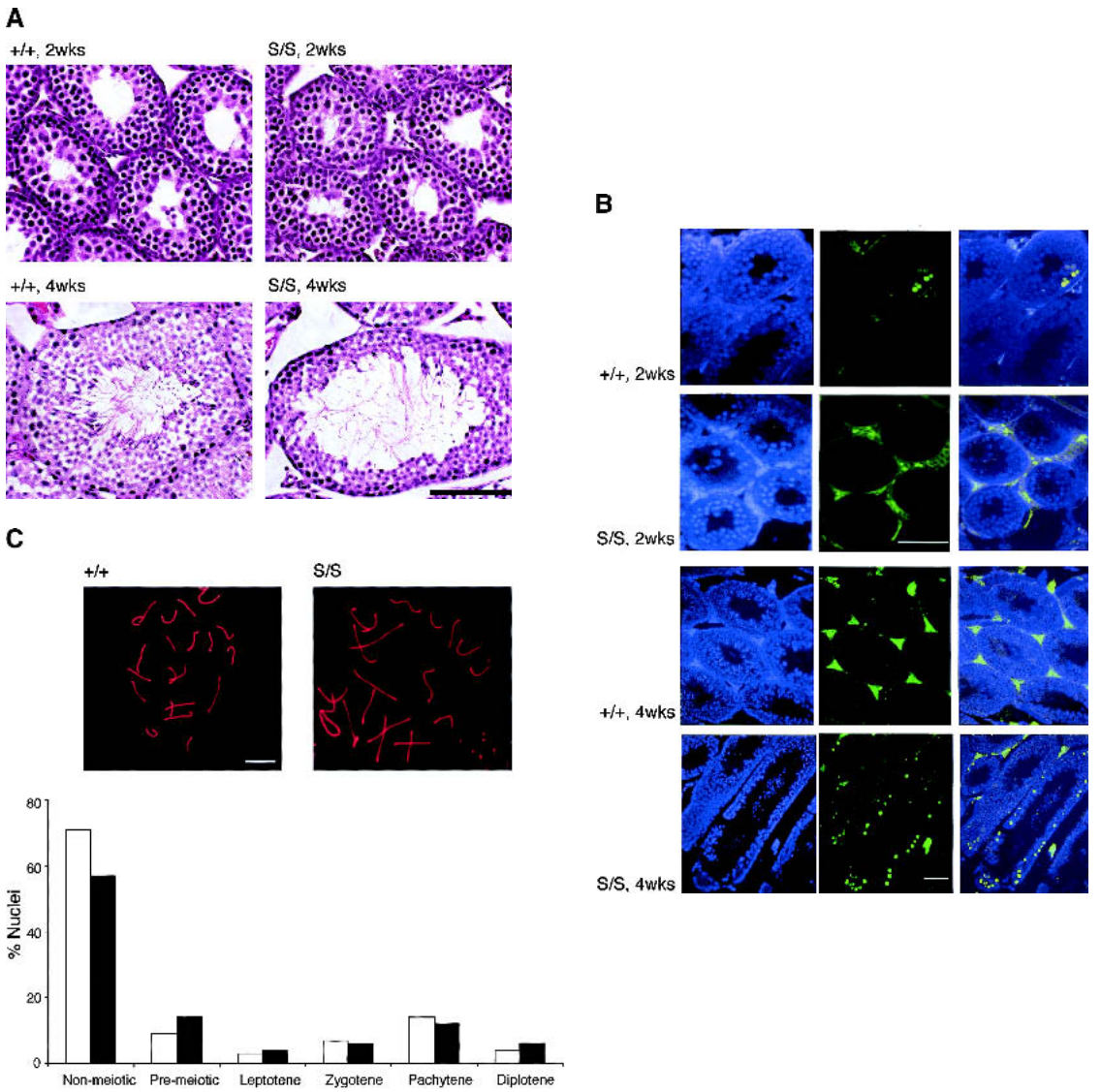

Figure 2. Progressive degeneration in *Rad50*$^{S/S}$ testes is not associated with meiotic recombination defects. (*A*) Hematoxylin and eosin (H&E) staining of testes sections from 2- and 4-wk-old *Rad50*$^{+/+}$ and *Rad50*$^{S/S}$ mice. Bar, 100 µm; magnification, 400×. (*B*) TUNEL-staining of apoptotic cells (FITC; green; *middle*) and nuclear counterstaining with DAPI (blue; *left*) in testes sections. Two-channel overlay of TUNEL-FITC and DAPI (*right*). Two-week-old sections, magnification 400×. Four-week-old sections, magnification 100×. Bars, 100 µm. (*C*) Surface-spread spermatocyte nuclei were stained with Cor1 antiserum, which recognizes Scp3 protein (red). Images of *Rad50*$^{+/+}$ and *Rad50*$^{S/S}$ spermatocyte nuclei in pachytene demonstrate normal chromosome pairing. Chromosomes from a second meiotic cell are seen in the lower right corner of the *Rad50*$^{S/S}$ image. Bar, 10 µm; magnification, 1000×. Graph, meiotic progression in ≥200 *Rad50*$^{+/+}$ (white bars) and *Rad50*$^{S/S}$ (black bars) nuclei determined by Cor1 staining patterns and chromosomal structure.

Cell transfer experiments were performed to determine whether *Rad50*$^{S/S}$ pathology was intrinsic to hematopoietic cells. Irradiated *Rad50*$^{S/S}$ mice were injected with wild-type fetal liver cells to assess the ability of *Rad50*$^{S/S}$ bone marrow stroma to support hematopoietic differentiation. Reconstitution of hematopoietic cells in *Rad50*$^{S/S}$ recipients of wild-type fetal liver was comparable to that in control recipients (Fig. 3C). PCR-based genotyping confirmed that wild-type cells were responsible for reconstitution of *Rad50*$^{S/S}$ mice (data not shown). In contrast, wild-type recipients of *Rad50*$^{S/S}$ fetal liver had 10–1000-fold fewer hematopoietic cells than controls at 6 wk after transfer (Fig. 3C). These data suggested that *Rad50*$^{S/S}$ bone marrow failure was attributable to hematopoietic failure independent of stromal defects.

To confirm that interpretation, we mixed wild-type and *Rad50*$^{S/S}$ fetal liver cells in a 1:1 ratio and transferred them into wild-type recipients. In this setting, *Rad50*$^{S/S}$ cells would be supported by the wild-type hematopoietic milieu during differentiation. Full reconstitution was evident 4 wk after transfer, and genotypic analysis

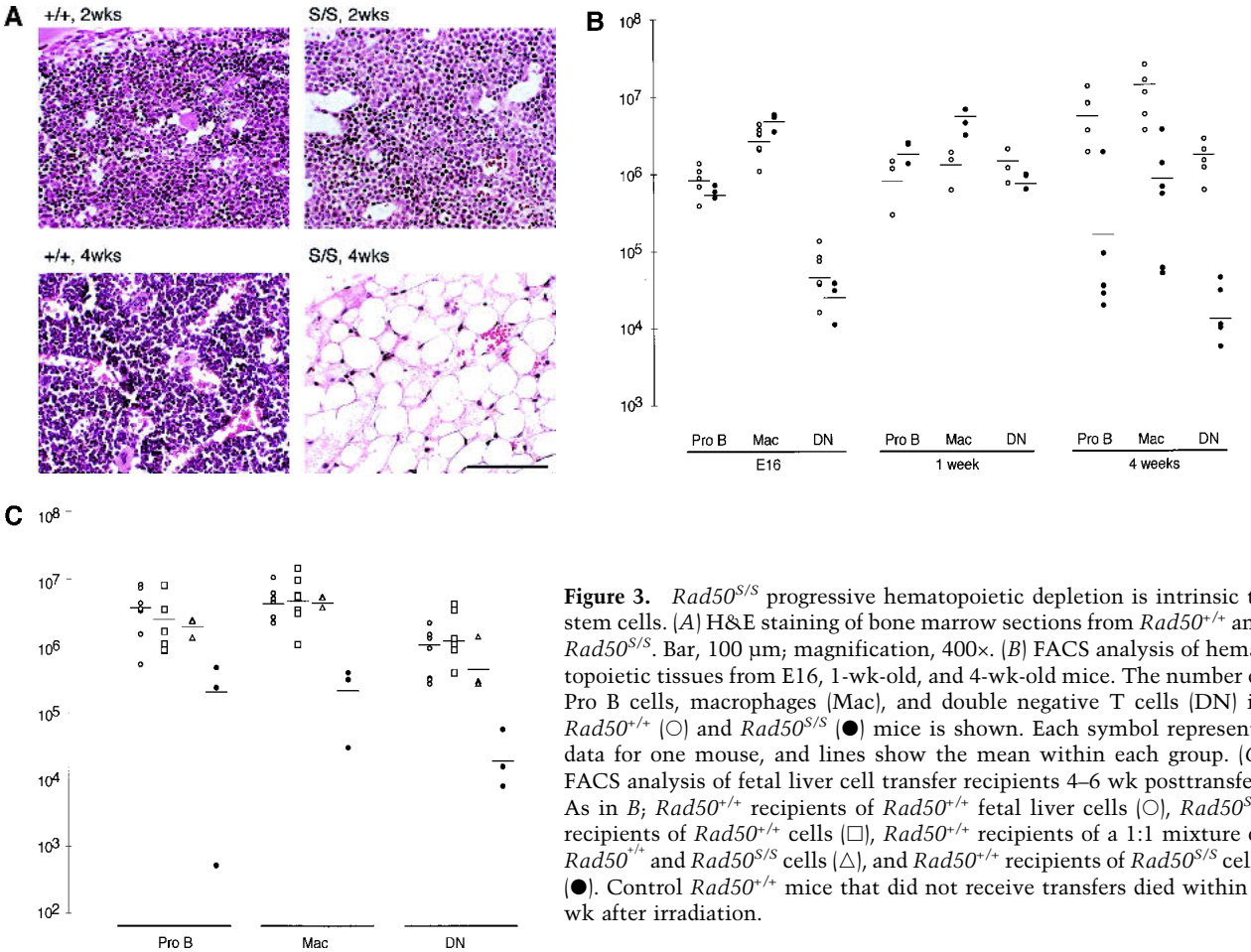

Figure 3. *Rad50*$^{S/S}$ progressive hematopoietic depletion is intrinsic to stem cells. (*A*) H&E staining of bone marrow sections from *Rad50*$^{+/+}$ and *Rad50*$^{S/S}$. Bar, 100 µm; magnification, 400×. (*B*) FACS analysis of hematopoietic tissues from E16, 1-wk-old, and 4-wk-old mice. The number of Pro B cells, macrophages (Mac), and double negative T cells (DN) in *Rad50*$^{+/+}$ (○) and *Rad50*$^{S/S}$ (●) mice is shown. Each symbol represents data for one mouse, and lines show the mean within each group. (*C*) FACS analysis of fetal liver cell transfer recipients 4–6 wk posttransfer. As in *B*; *Rad50*$^{+/+}$ recipients of *Rad50*$^{+/+}$ fetal liver cells (○), *Rad50*$^{S/S}$ recipients of *Rad50*$^{+/+}$ cells (□), *Rad50*$^{+/+}$ recipients of a 1:1 mixture of *Rad50*$^{+/+}$ and *Rad50*$^{S/S}$ cells (△), and *Rad50*$^{+/+}$ recipients of *Rad50*$^{S/S}$ cells (●). Control *Rad50*$^{+/+}$ mice that did not receive transfers died within 2 wk after irradiation.

showed that wild-type, but not *Rad50*$^{S/S}$ cells, were present in hematopoietic tissues of reconstituted animals (Fig. 3C; data not shown). Thus, the presence of wild-type hematopoietic cells and stroma did not increase the ability of *Rad50*$^{S/S}$ stem cells to reconstitute hematopoietic compartments. These experiments indicated that progressive bone marrow depletion in *Rad50*$^{S/S}$ mice was primarily attributable to hematopoietic stem cell failure.

Normal V(D)J recombination in Rad50$^{S/S}$ *mice*

DNA hairpins are intermediates in the site-specific recombination process required for antigen receptor gene assembly, V(D)J recombination (Roth et al. 1992; McBlane et al. 1995). Recent in vitro experiments suggest that the artemis/DNAPK complex may open V(D)J hairpins (Ma et al. 2002). However, in light of in vitro and in vivo data, the possibility remains that the Mre11 complex may also influence this process (Paull and Gellert 1998, 1999; Lobachev et al. 2002). We used ligation-mediated PCR to assess whether hairpin opening was defective in *Rad50*$^{S/S}$ mice (Zhu and Roth 1995). TCR Dδ2 hairpins were readily detected in thymus DNA from 1-wk-old *scid* mice; however none were detected in *Rad50*$^{S/S}$ samples (Fig. 4).

Quantitative PCR showed that in vivo V to DJ and D to J rearrangement frequencies, as well as the structure of the joints formed, were normal in E16 and in 4-wk-old *Rad50*$^{S/S}$ mice (data not shown). Transient V(D)J recombination assays indicated that coding and signal joints were formed at comparable frequencies in wild-type and *Rad50*$^{S/S}$ MEFs (recombination frequency for signal joints: 0.12% in wild-type, 0.29% in *Rad50*$^{S/S}$; coding joints: 0.5% in wild-type, 1.2% in *Rad50*$^{S/S}$), and like *Rad50*$^{S/S}$ in vivo joints, did not exhibit abnormal structures (data not shown). These data indicate that V(D)J recombination was normal in *Rad50*$^{S/S}$ mice, and suggest that hairpin opening during V(D)J recombination is not impaired by the *Rad50*^{K22M} mutation.

p53 deficiency mitigates the Rad50$^{S/S}$ *phenotype*

The correlation of age with malignancy, together with the observation that testes and bone marrow showed age-dependent cellular attrition, suggested that the *Rad50*^{K22M} mutation caused chronic genotoxic stress. Because p53 profoundly influences genotoxic stress responses (Prives and Hall 1999), we hypothesized that p53 deficiency would mitigate the *Rad50*$^{S/S}$ phenotype. Conversely, because potentially oncogenic genetic alter-

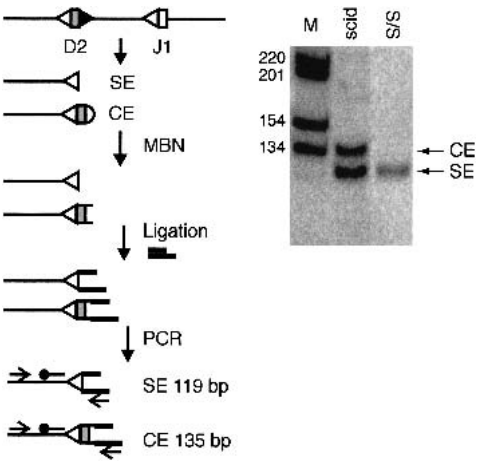

Figure 4. Normal hairpin resolution in *Rad50$^{S/S}$* thymocytes. Hairpin coding ends (CE), oligonucleotides were ligated to the D2/J1 blunt signal ends (SE) and the open CEs. Ends were PCR amplified using Dδ2– and oligospecific primers (arrows), and products were detected using the probe shown (line with a circle). Expected sizes of PCR products are indicated. Blot, LMPCR of 1 μg of MBN-treated thymic DNA from *scid* and *Rad50$^{S/S}$* mice. M, radiolabeled size marker; sizes (bp) shown on *left*.

ations would accumulate without inducing apoptosis in p53-deficient *Rad50$^{S/S}$* mice, we expected Rad50S to reduce the tumor latency of *p53$^{-/-}$* animals.

Indeed, reduced p53 dosage partially rescued Rad50S-dependent depletion in the hematopoietic compartment, and the *Rad50^{K22M}* mutation accelerated *p53$^{+/-}$* and *p53$^{-/-}$* tumorigenesis (Fig. 5A,B). B cell numbers were increased 3–10-fold and 5–20-fold above *Rad50$^{S/S}$* levels in *p53$^{+/-}$ Rad50$^{S/S}$* and *p53$^{-/-}$ Rad50$^{S/S}$* mice, respectively. Macrophages were threefold increased and T cells were 3–20-fold increased in both *p53$^{+/-}$ Rad50$^{S/S}$* and *p53$^{-/-}$ Rad50$^{S/S}$* mice (cf. Figs. 3B and 5A). The partial rescue of hematopoietic cell survival in *p53$^{+/-}$ Rad50$^{S/S}$* and *p53$^{-/-}$ Rad50$^{S/S}$* mice was associated with increased lifespan (Fig. 5B). *Rad50^{K22M}* significantly altered *p53$^{+/-}$* and *p53$^{-/-}$* tumor susceptibility. *p53$^{+/-}$* control mice in our colony developed osteosarcomas after 12 mo of age (N = 34), whereas *p53$^{+/-}$ Rad50$^{S/S}$* mice died from thymic lymphomas at an average of 5 mo (N = 17; $P = 0.002$). *p53$^{-/-}$ Rad50$^{S/S}$* animals (N = 7, average age of death 3.3 mo; $P = 0.05$) died earlier than *p53$^{-/-}$* mice (N = 17, average age of death 4.5 mo) without changes in *p53$^{-/-}$* tumor spectrum (Jacks et al. 1994). In contrast to *Rad50$^{S/S}$* animals, the double mutants succumbed to lymphoma and did not show overt signs of anemia.

p53 deficiency also suppressed the attrition of cells in the seminiferous tubules, correlated with abrogation of testicular apoptosis in both *p53$^{+/-}$ Rad50$^{S/S}$* and *p53$^{-/-}$ Rad50$^{S/S}$* mice (Fig. 5C). The suppression of testicular apoptosis raised the possibility that defects in meiotic recombination, obscured by apoptotic attrition in p53-proficient cells, would be evident in double mutants. However, *p53$^{+/-}$ Rad50$^{S/S}$* and *p53$^{-/-}$ Rad50$^{S/S}$* males did not exhibit an arrest in meiotic progression, nor were aberrant chromosomal structures detected (data not shown). These data indicate that apoptosis in *Rad50$^{S/S}$* testes was not associated with meiotic recombination defects.

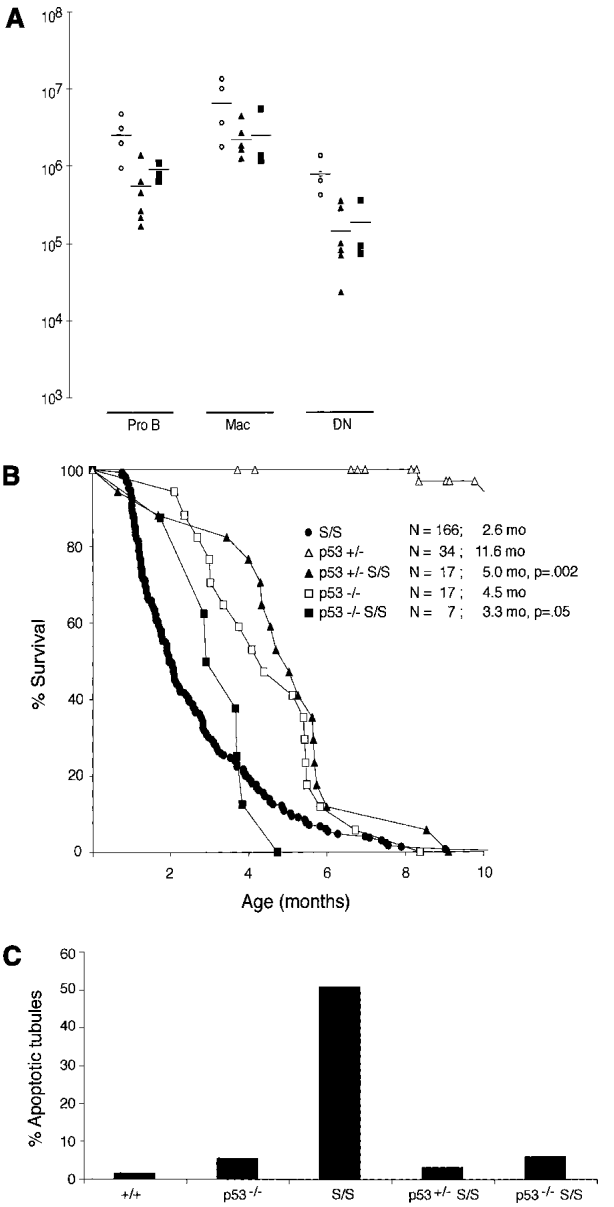

Figure 5. p53 deficiency partially rescues the *Rad50$^{S/S}$* phenotype. (*A*) FACS analysis of 4-wk-old 129/SvEv *Rad50$^{+/+}$* (○), *p53$^{+/-}$ Rad50$^{S/S}$* (▲), and *p53$^{-/-}$Rad50$^{S/S}$* (■) mice; depicted as in Fig. 3B. (*B*) Mouse survival. Each data point represents the fraction of surviving mice at a given age in months. N, total number of mice for each genotype. Only autopsied mice are included. The average age of death in months (mo) is shown for each genotype with the *P*-value compared to the relevant control determined by the Wilcoxon rank sum test. (*C*) Results from TUNEL staining of testes sections from 4-mo-old mice. The % apoptotic tubules is the average fraction of tubules with ≥4 apoptotic cells in serial sections from two mice of each genotype.

Chronic genotoxic stress in cells from Rad50$^{S/S}$ *mice*

The rescue of *Rad50*$^{S/S}$ hematopoietic and testicular attrition and the reduced tumor latency in *p53*$^{+/-}$ *Rad50*$^{S/S}$ and *p53*$^{-/-}$ *Rad50*$^{S/S}$ mice supported the interpretation that chronic genotoxic stress was the underlying cause of the *Rad50*$^{S/S}$ phenotype. Indices of genotoxic stress were assessed in primary cell cultures. First, the apoptotic indices of wild-type and *Rad50*$^{S/S}$ MEFs were analyzed by FACS. Compared to wild-type controls, unirradiated *Rad50*$^{S/S}$ MEFs exhibited a 1.4–3.4-fold increase in the fraction of cells with sub-G1 DNA content. A similar increase in annexinV staining was also found in unirradiated *Rad50*$^{S/S}$ MEFs. The increase in apoptotic cells after irradiation (IR) was similar in *Rad50*$^{S/S}$ and control cells, indicating that the apoptotic response to IR was not compromised (Table 1).

Second, the presence of phosphorylated histone H2AX (γ-H2AX), which is correlated with the presence of DNA damage (Rogakou et al. 1999; Paull et al. 2000; Ward and Chen 2001), was examined in MEFs by immunofluorescence and flow cytometry with γ-H2AX antiserum. The percentage of γ-H2AX-positive cells was increased in unirradiated *Rad50*$^{S/S}$ cells to levels comparable to that in wild-type irradiated cells (Table 1).

Finally, since the mammalian Mre11 complex localizes to sites of DNA replication (Maser et al. 2001), sites of DNA damage (Nelms et al. 1998; Mirzoeva and Petrini 2001), and to human telomeres (Zhu et al. 2000), we reasoned that attenuation of Mre11 complex function at any one of these venues could induce chromosome aberrations in *Rad50*$^{S/S}$ cells. To address this possibility, spectral karyotype (SKY) and conventional karyotypic analyses were performed. Increased levels of chromosome breaks were evident in ear fibroblast cultures established from *Rad50*$^{S/S}$ and *p53*$^{-/-}$ *Rad50*$^{S/S}$ mice (Table 2; Fig. 6A). Increases in chromosome breaks and rearrangements were also detected in SV40-transformed *Rad50*$^{S/S}$ ear fibroblasts by conventional analysis of Giemsa-stained metaphase cells (Table 2). These data were consistent with the interpretation that the *Rad50*^{K22M} mutation exerted an impact on chromosome stability.

Because the events that lead to depletion of hematopoietic cells also predispose malignancy, the mechanistic basis of *Rad50*$^{S/S}$ pathology should be evident in tumors from these mice. *Rad50*$^{S/S}$ and *p53*$^{-/-}$ *Rad50*$^{S/S}$ thymic lymphoma cells exhibited increased chromosomal instability in SKY analysis (Table 3; Fig. 6B). Compared to *p53*$^{-/-}$ tumors, most *Rad50*$^{S/S}$ and *p53*$^{-/-}$ *Rad50*$^{S/S}$ tumors had more chromosome rearrangements and some exhibited an increased frequency of nonclonal karyotypes, suggesting that events leading to instability were ongoing (Table 3).

Giemsa-stained chromosomes from tumors revealed similar karyotypic instability. Notable was a significant increase in short-arm chromosome fusions (Table 4). Fluorescent in situ hybridization (FISH) with a CCCTAA probe was performed to determine whether fusions in *Rad50*$^{S/S}$ cells resulted from joining of telomeric or interstitial DNA. The majority of short-arm fusions in *Rad50*$^{S/S}$ and *p53*$^{-/-}$ *Rad50*$^{S/S}$ tumors contained two intense telomeric signals at the join, indicating that telomeric DNA was retained in these fusions (Fig. 6C). Fusions containing telomeric DNA were detected by FISH in all *Rad50*$^{S/S}$ and *p53*$^{-/-}$ *Rad50*$^{S/S}$ tumors, but not in *p53*$^{-/-}$ tumors (Table 4). These data raise the possibility that telomere failure was among the chromosomal phenotypes associated with the *Rad50*^{K22M} mutation, and collectively support the interpretation that *Rad50*$^{S/S}$ cells are subject to chronic genotoxic stress.

Table 1. *Genotoxic stress in* Rad50$^{S/S}$ *cells*

		Cytology	FACS				
Sample	Genotype	% γ-H2AX+ O Gy	% γ-H2AX+ 0 Gy	% γ-H2AX+ 12 Gy	% sub G1 0 Gy	% Annexin+ 0 Gy	% Annexin+ 12 Gy
1960-3,5	*Rad50*$^{+/+}$	23, 25	0.58	0.73	1.00	0.5	1.7
1960-8	*Rad50*$^{S/S}$	33, 43	1.27	3.14	1.40	0.9	2.5
fold[a]		+1.6	+2.2	+4.3	+1.4	+1.7	+1.4
193-11	*Rad50*$^{+/+}$	39, 34	0.45	0.79	1.34	ND	ND
9033-3,8	*Rad50*$^{S/S}$	47, 51	0.67	1.19	2.54	ND	ND
fold		+1.5	+1.5	+1.5	+1.9		
12317-5,6	*Rad50*$^{+/+}$	ND	1.1	ND	2.5	6	8
14205-6,7	*Rad50*$^{S/S}$	ND	1.9	ND	8.5	12	14
fold			+1.7		+3.4	+2.0	+1.8

For cytology, passage 2 (p2) MEFs were grown on cover slips, extracted, fixed, and stained with antisera to γ-H2AX. Data are from two independent cultures from which ≥150 cells were analyzed. % γ-H2AX+ represents the fraction of cells with ≥3 nuclear γ-H2AX foci or complete nuclear staining.

For FACS, mock-treated or irradiated p2 MEFs were fixed after 1 h and stained with antisera to γ-H2AX or propidium iodide (PI) and unfixed cells were stained 24 h later for annexin V. Data are the average of three independent cultures from which 10,000 cells each were analyzed. % γ-H2AX+ shown is the % of cells with the most γ-H2AX+ staining determined by fluorescence intensity. % sub G1 represents cells with less than 2N DNA content determined by PI staining.

[a]The fold increase in unirradiated *Rad50*$^{S/S}$ cells vs. *Rad50*$^{+/+}$ cells (fold) was significant ($p < 0.05$) for each experiment as determined by Fisher's exact test. ND, not determined.

Table 2. *Karyotypic analysis of ear fibroblast cultures*

Sample[a]	Genotype	Chr	+/–		Breaks	Rearrangements	N
12221 p3	+/+	40	0/0			0	8
		41	1/0			0	2
				total	0	0	10
12053 p3	*Rad50*$^{S/S}$	40	0/0			0	9
		38	0/1			1	1
				total	12	1	10
11195 p3	*p53*$^{-/-}$	40	0/0			0	10
		40	1/1			0	1
				total	0	0	11
11195p10	*p53*$^{-/-}$	47-77	1/19			0	8
		47-77	1/19			1	1
		47-77	1/19			2	1
				total	0	3	10
6415p10	*p53*$^{-/-}$ *Rad50*$^{S/S}$	80	0/0			0	1
		35-82	1-4/1-9			0	10
		35	1/6			1	1
		107	28/0			0	1
				total	2	1	13

Sample[b]	Genotype	Chr	+/–	Breaks	Rearrangements[c]	N
11683	*SV40* +/+	ND	ND	7	5	115
11685	*SV40 S/S*	ND	ND	17	22	124

[a]Spectral karyotyping was performed on metaphase cells from primary ear fibroblast cultures at passage numbers indicated (p). Breaks were nonclonal and are shown as a total from all metaphases of each sample.
[b]Chromosome aberrations were scored on Giemsa-stained metaphase spreads from nonclonal SV40-transformed ear fibroblast populations.
[c]Rearrangements reflect the sum of exchanges and chromosome fusions.
Chr, chromosome number; +/–, number of chromosomes gained (+) or lost (–); N, number of cells examined; ND, not determined.

Discussion

The Mre11 complex is integral to a diverse spectrum of functions that bear upon chromosome stability. Genetic analyses in *S. cerevisiae* establish that the complex's influence can be generally attributed to either structural roles, which primarily influence the DNA recombination functions of the complex, or enzymatic (nucleolytic) roles, which appear to influence DSB end processing or degradation of certain DNA structures. The complex's structural role has been invoked to account for the inability of null Mre11 complex mutants to utilize sister chromatids during recombinational DNA repair, whereas nuclease-deficient mutants do not exhibit this property (Ivanov et al. 1992; Moore and Haber 1996; Bressan et al. 1999). A molecular basis for such a role is suggested by electron microscopic studies of the human Mre11 complex and structural analysis of the *Pyrococcus furiosis* Mre11 complex. Those data indicate that the complex may bridge DNA ends or sister chromatids via the coiled coil regions of Rad50 (de Jager et al. 2001; Hopfner et al. 2002). The in vivo role of the complex's nuclease functions have been inferred from the *S. cerevisiae S* alleles, in which the initial processing of meiotic DSBs is impaired, and from the synthetic lethality of nuclease-deficient mutants with Rad27 deficiency (Symington 1998; Debrauwere et al. 2001).

We determined previously that a null *Rad50* mouse mutant, in which the structural role of the Mre11 complex is presumably abrogated, is inviable (Luo et al. 1999). Therefore, we established a *Rad50*$^{S/S}$ mouse mutant in which the Mre11 complex is intact, but functionally hypomorphic. In contrast to Rad50-deficient mice, *Rad50*$^{S/S}$ mice exhibit only partial embryonic lethality. *Rad50*$^{S/S}$ mice have shortened lifespan associated with progressive loss of cells in the male germ line and in hematopoietic lineages, and die with hematopoietic failure by 3 mo of age. Sporadically appearing longer-lived *Rad50*$^{S/S}$ animals are highly predisposed to malignancy. Underlying these phenotypic outcomes is the accumulation of chromosome aberrations. In p53-proficient mice, these events precipitate the cellular attrition observed, whereas in the context of p53 deficiency, abrogation of apoptosis diminishes cellular attrition but dramatically enhances tumorigenesis.

Progressive attrition of hematopoietic and spermatogenic lineages in Rad50$^{S/S}$ *mice*

Rad50$^{S/S}$ pathology is largely restricted to hematopoietic and germ cell lineages. Fetal liver cell transfer experiments demonstrated that the progressive hematopoietic failure observed is correlated with depletion of stem cells. An analogous progenitor depletion may underlie

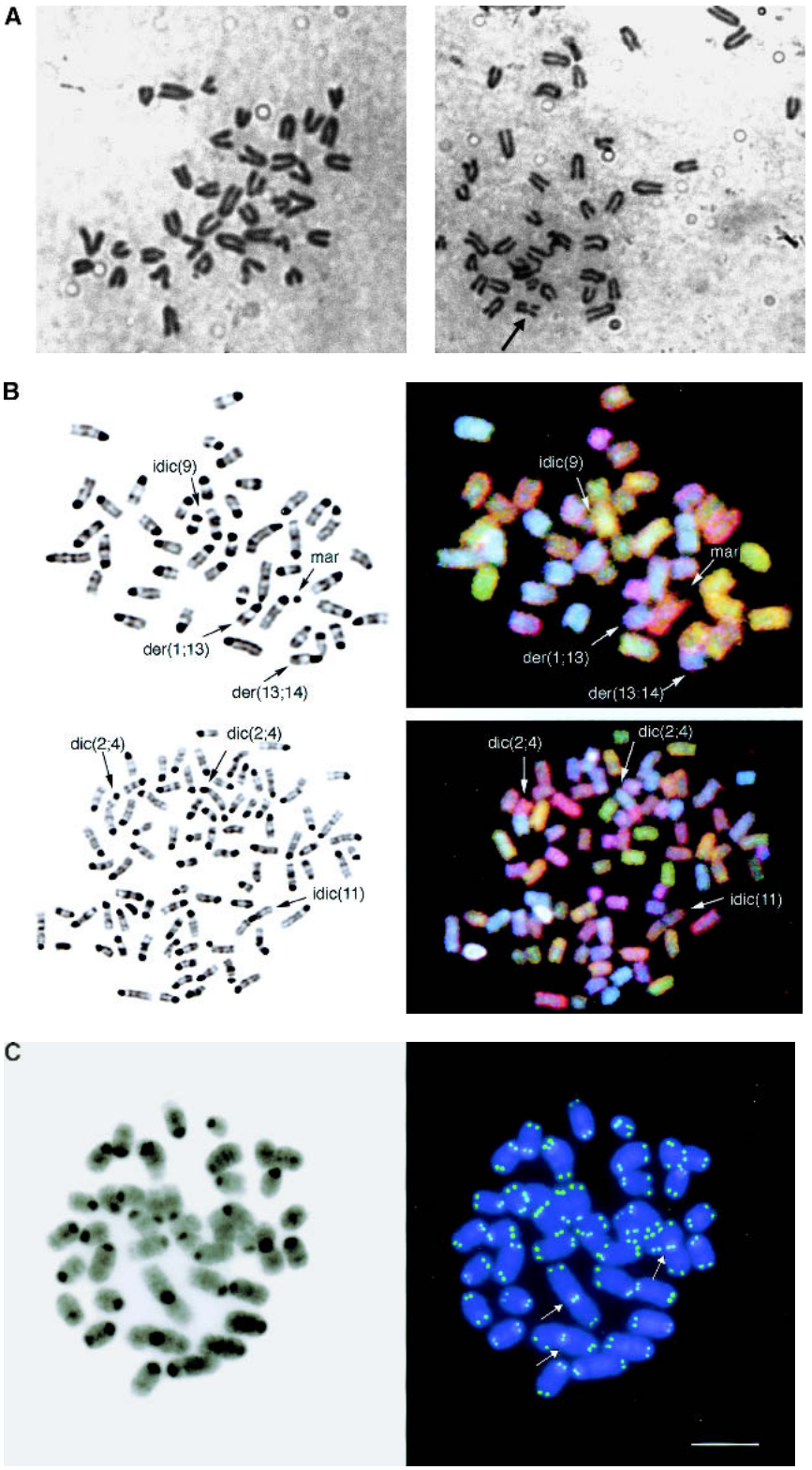

Figure 6. Chromosome instability in *Rad50*$^{S/S}$ cells. (*A*) Images of Giemsa-stained metaphase cells. (*Left*) a normal metaphase spread from a *Rad50*$^{S/S}$ ear fibroblast. (*Right*) *Rad50*$^{S/S}$ ear fibroblast metaphase with one broken chromosome (arrow). Magnification, 1000×. (*B*) SKY analysis of thymic lymphoma cells. Metaphase cells from *p53*$^{-/-}$*Rad50*$^{S/S}$ (*upper panel*, tumor 5390) and *Rad50*$^{S/S}$ (*lower panel*, tumor 5587) tumors. (*Left*) Inverted image of the metaphase cells counterstained with DAPI. (*Right*) Spectral image of the metaphase cells. The structurally rearranged chromosomes are identified with arrows, and include short-arm fusions [der(13;14) and der(1;13)], an isodicentric fusion [idic(9)], and a small marker chromosome of unknown origin [mar] in the *p53*$^{-/-}$*Rad50*$^{S/S}$ tumor, as well as dicentric and isodicentric rearrangements [dic(2;4) and idic(11)] in the *Rad50*$^{S/S}$ tumor. (*C*) (*Right*) Two-channel image of a representative metaphase spread from a *p53*$^{-/-}$*Rad50*$^{S/S}$ lymphoma subjected to FISH using an FITC-conjugated telomeric probe (green) and counterstained with DAPI (blue). (*Left*) Inverted DAPI image of the metaphase cell. Bar, 10 μm; magnification, 1000×.

the progressive attrition of cells in the seminiferous tubules, because meiotic progression is not impaired by Rad50S. In this regard, the *Rad50*$^{S/S}$ mice are similar to late-generation telomerase-deficient (*mTR*$^{-/-}$) mice, which experience telomere failure as a sequela to telomere shortening, and exhibit relatively selective depletion of hematopoietic and spermatogenic cells (Lee et al. 1998; Herrera et al. 1999).

Chronic genotoxic stress associated with the *Rad50*^{K22M} allele would differentially affect hematopoi-

Table 3. *Spectral karyotype analysis of thymic lymphomas*

Sample	Genotype	Chr	+/–		Rearrangements	N
AN1	$p53^{-/-}$	61	21/0		0	9
		46	6/0		0	1
		49	9/0		0	1
				total	0	11
6141	$p53^{-/-}$ $Rad50^{+/S}$	76	5/9	total	1	8
5492	$Rad50^{S/S}$	42	3/1		0	7
		42	4/2		0	2
		44	5/1		1	1
		37	3/6		2	1
		42	5/3		0	1
		49	12/3		0	1
		43	4/1		0	1
				total	3	14
5587	$Rad50^{S/S}$	78	6/6		2	9
		40	0/0		0	1
				total	18	10
6175	$Rad50^{S/S}$	41	1/0		0	3
		80	0/0		0	4
		40	0/0		0	4
				total	0	11
5390	$p53^{-/-}$ $Rad50^{S/S}$	41	2/0		2	2
		39–40	1/1		3	3
		40–43	3/1		2	3
		42	3/0		1	1
		42	5/1		2	1
				total	22	10

The number of chromosome aberrations in tumor cultures determined by spectral karyotyping is shown. Chr, chromosome number; +/–, number of chromosomes gained (+) or lost (–); N, number of cells examined.

etic and spermatogenic tissues for two reasons. First, in contrast to other proliferative tissues such as intestine or skin, they arise from extensive proliferation of a relatively small number of stem cells and committed precursors (Weissman 2000). Therefore, for each stem or precursor cell depleted, a relatively large proportion of the tissue—arising from geometric expansion from the depleted stem cell—would be lost. Second, decreased cellularity, as a primary outcome of stem cell depletion and the ensuing reduction in differentiated cells, imposes increased proliferative demand on the residual population. Whereas mutations that result in gross chromosomal instability would have broad pathological outcomes, less severe mutations would more specifically affect tissues that rely upon limited precursor populations.

The selective effect of $Rad50^{K22M}$ on hematopoietic and spermatogenic tissue is thus consistent with the observation that the magnitude of chromosomal instability in $Rad50^{S/S}$ mice was relatively low. The chromosomal aberrations seen in $Rad50^{S/S}$ and $p53^{-/-}$ $Rad50^{S/S}$ lymphomas were not seen in $p53^{-/-}$ tumors, and were largely clonal, indicating that these chromosomal aberrations are unique to the $Rad50^{K22M}$ allele, and further, that they accumulate at a relatively low rate. Were $Rad50^{S/S}$ mice longer-lived, a broader spectrum of pathology would likely emerge. By analogy, whereas hematopoietic and spermatogenic depletion are seen first in late-generation $mTR^{-/-}$ mice, an aged cohort of these mice exhibited much broader pathology, including skin and intestine defects (Herrera et al. 1999; Rudolph et al. 1999).

Murine Rad50S *alleles*

The inability of $Rad50^{K6E}$ and $Rad50^{R83I}$ to support cell viability was not predicted from the behavior of the corresponding *S. cerevisiae* mutants. Given the conservation of Mre11 and Rad50, it is unlikely that the enzymatic functions impaired by the murine *S* mutations differ from those in *S. cerevisiae*. Assuming that the three *S* mutations examined impair the same functions, the inviability of $Rad50^{K6E}$ and $Rad50^{R83I}$ could simply reflect a more severe form of the $Rad50^{K22M}$ phenotype, in which cell death ensues from greater increase in the levels of chromosome instability. It is also conceivable that increased severity could result from defects in processing a more diverse spectrum of substrates in $Rad50^{K6E}$- and $Rad50^{R83I}$-expressing cells.

The lack of meiotic recombination and V(D)J recombination defects in $Rad50^{K22M}$ mutants, which was also unexpected, could be explained by the same argument. *S* mutations that exert a profound effect on meiotic progression would be inviable. Although a meiotic arrest was not clearly evident in the $Rad50^{K22M}$ mice, a subtle defect might not have been detected by our analysis.

The Mre11 complex: Diverse mechanisms in maintaining genomic integrity

Mutations in *MRE11* and *NBS1* are associated with cancer predisposition, chromosome instability, and cell cycle checkpoint defects in A-TLD and NBS (Carney et al. 1998; Stewart et al. 1999). Despite their severe clinical and cellular phenotypes, those mutations do not confer overt recombinational DNA repair defects, as was true in $Rad50^{S/S}$ mice. In contrast, null Mre11 complex mutations, which cause profound DNA recombination defects in *S. cerevisiae*, are lethal in vertebrates. These outcomes support the possibility that essential and nonessential Mre11 complex functions are mechanistically distinct. The *P. furiosis* Mre11/Rad50 complex suggests a molecular basis for distinct mechanisms. This complex contains a bifunctional DNA binding domain in which the active site of the Mre11 nuclease is capable of binding ssDNA, whereas an adjacent site accommodates double-stranded DNA. Occupancy of the sites is mutually exclusive, suggesting that a given interaction with DNA facilitates enzymatic (in the ssDNA binding domain) or structural (in the dsDNA binding domain) functions (Hopfner et al. 2001). The data presented here argue that the essential functions of the complex cannot be clearly divided according to its enzymatic or structural roles.

Table 4. *Chromosome aberrations in thymic lymphomas*[a]

Tumor	Genotype	Fragments	Breaks	Exchanges[b]	End-to-end[c]	Short arm[d]	N[e]	Telomeric fusion[f]
8200	*p53*$^{-/-}$	1.0	0	0.3	0	0.1	50 (80)	ND
AN1	*p53*$^{-/-}$	0.1	0.1	0.4	0.1	0.2	51 (43)	ND
6141	*p53*$^{-/-}$ *Rad50*$^{+/S}$	3.5	0.2	0.5	0	0.2	54 (100)	0
5492	*Rad50*$^{S/S}$	0.4	0.1	0.2	0.1	0.1	60 (43)	0.2
5587	*Rad50*$^{S/S}$	0.1	0.1	0.3	0	0.3	60 (38)	0.1
6175	*Rad50*$^{S/S}$	0.6	0.3	0.4	0.1	0	50 (62)	0.1
5390	*p53*$^{-/-}$ *Rad50*$^{S/S}$	0.2	0	0.2	0.1	3.1[g]	54 (100)	2.1[g]
6256	*p53*$^{-/-}$ *Rad50*$^{S/S}$	0.3	0	0.2	0.2	1.1[g]	48 (79)	0.7[g]
6531	*p53*$^{-/-}$ *Rad50*$^{S/S}$	0.2	0.1	0.1	0	0.4[g]	50 (40)	0.2[g]

[a]Determined by phase contrast analysis.
[b]Long-arm chromatid fusions.
[c]Long-arm chromosome fusions.
[d]Short-arm chromosome fusions.
[e]Number of metaphase cells examined (% with at least one aberration).
[f]Fusions (including exchanges, end-to-end, and short-arm fusions) per metaphase with telomeric DNA retained; determined in a separate experiment in which FISH was performed with a telomeric repeat probe. ND, not done.
[g]$p < 0.05$ when compared to *p53*$^{-/-}$ tumors using the Wilcoxon rank sum test.

Finally, the data clearly indicate that the Mre11 complex exerts a profound influence on homeostasis in mammalian tissues even when its checkpoint and DNA recombination functions are not overtly impaired. The *Rad50*$^{S/S}$ mouse therefore establishes that subtle hypomorphism in a DNA damage response pathway is sufficient to induce severe pathology. This observation has important implications for understanding the mechanistic basis of disease related to chromosomal metabolism.

Materials and methods

Analysis of Rad50S *alleles*

Missense amplification of *Rad50* cDNA from *pmRad50* (Luo et al. 1999) using the primers mR50–24S (5′-GATAGAGGATAAAGATATGCAGATTATCTCTTTC-3′) and mR50–24A (5′-GAAAGAGATAATCTGCATATCTTTATCCTCTATC-3′), mR50–26S (5′-CGGGCCCAGATTATCTTGCAGTTTCGAGATG-3′) and mR50–26A (5′-CATCTCGAAACTGCAAGATAATCTGGGCCCG-3′), or mR50–27S (5′-TCCCGGATCGAAGAGATGAGCATTC-3′) and mR50–27A (5′-GAATGCTCATCTCTTCGATCCGGGA-3′) resulted in *pRad50*^{K22M}, *pRad50*^{R83I}, and *pRad50*^{K6E}, respectively. *pPGKhygro-Cre* was created by ligation of the *pBS185* (GIBCO-BRL) *Hind*III *Cre* fragment into *pPGKhyg* (Mortensen et al. 1991). Hygromycin- and gancyclovir-resistant clones from *mRad50*^{Brdm1}/ *mRad50*^{Brdc1} ES cells co-electroporated with 30 μg of *Kpn*I-linearized *pPGKhygro-Cre* and 200 μg of an *Afl*II-linearized *Rad50* cDNA were analyzed by Southern blotting as described (Luo et al. 1999).

Derivation of mutant mice

Details of the *pkin-24ploxp* targeting vector construction will be furnished upon request. Following transfection of Ab2.2 ES cells and selection, targeted clones were identified by Southern blot. Blastocyst injections and derivation of chimeric mice were done by standard methods. Chimeras were mated with C57Bl6 mice (Harlan Sprague Dawley) or 129/SvEv mice (Taconic) for 129/SvEv. *Rad50*$^{S/S}$ mice in mixed and pure 129/SvEv backgrounds had the same phenotype. *Tgn CMV-Cre* transgenic mice (Nagy et al. 1998) were mated with *Rad50*$^{+/K22M}$ mice to derive *Rad50*$+^{K22Mcre/K22Mcre}$ mice. p53-deficient mice (Jacks et al. 1994) and double mutants were maintained on a 129/SvEv background. Details of genotyping *Rad50*$^{S/S}$ mice are available upon request.

Cell derivation and culture

E14.5 MEFs were maintained in DMEM/10% fetal bovine serum (FBS)/L-glutamine (GIBCO) with routine 1:3 passages. Ear fibroblasts obtained from the dorsal portion of one ear were minced, rinsed twice with PBS containing kanamycin (100 μg/mL), incubated at 37°C for 45 min in collagenase D/dispase neural protease from Bacillus polymyxa grade II (4 mg/mL each in DMEM, Boehringer Mannheim), and resuspended in DMEM/10% FBS with 5× PenStrep overnight. Filtered cells were plated and reached confluence before continued maintenance with 1:2 passages. Fugene 6 (Roche) was used to transfect cells with a variant of the SV40 DNA *pX-8* (Fromm and Berg 1982) containing an XhoI linker in the origin palindrome to derive transformed cells. Thymic lymphoma single cell suspensions were cultured in 90% RPMI 1640 (GIBCO)/10% FBS/1 ng/mL recombinant mouse interleukin-2 and interleukin-7 (Sigma)/PenStrep.

Protein analysis

Immunologic methods were as described (Dolganov et al. 1996) with Nbs1 (93–3; Williams et al. 2002).

DNA damage sensitivity assays

Sensivity was determined by colony formation essentially as described (Williams et al. 2002). Five thousand cells were treated for 2–3 h with etoposide (0–10 μg/mL), mitomycin C (0–3 μg/mL), or hydroxyurea (0–50 mM). The surviving fraction was determined after 7 d by colony forming ability. The radioresistant DNA synthesis assay was as described (Lim et al. 2000) except that MEFs were pulsed for 30 min with [^{3}H]thymidine 1 h post-IR with 10 Gy. Ionizing radiation-induced foci assays were as described (Maser et al. 1997). H2AX staining for immunofluorescence was performed on passage 2 MEFs using γ-H2AX-specific antiserum (Upstate Biotechnology; 1:1000) fol-

lowing in situ fractionation (Mirzoeva and Petrini 2001). For FACS, passage 2 MEFs were prepared 1 h after 0 or 12 Gy IR using the Cytofix/Cytoperm Staining Kit according to the manufacturer's directions (Pharmingen) and stained with γ-H2AX-specific antiserum (Upstate Biotechnology; 1:400) and anti-rabbit-FITC (Jackson Labs; 1:100) as described (J. Karlseder, O.K. Mirzoeva, B.R. Williams, J.H.J. Petrini, and T. de Lange, in prep.). Sub-G1 DNA content was determined for passage 2 MEFs fixed 1 h after 0 or 12 Gy IR using the Cytofix/Cytoperm Staining Kit according to the manufacturer's directions (Pharmingen), and stained with γ-H2AX-specific antiserum (Upstate Biotechnology; 1:1400) and anti-rabbit-FITC (Jackson Labs; 1:100; J. Karlseder, O.K. Mirzoeva, B.R. Williams, J.H.J. Petrini, and T. de Lange, in prep.) AnnexinV-FITC staining on unfixed passage 2 MEFs 24 h after 0 or 12 Gy was performed according to the manufacturer's directions (Sigma). All FACS data were analyzed with CellQuest software.

Histological analyses

Ten percent buffered formalin-fixed tissues were processed at the University of Wisconsin Veterinary School Histopathology Lab or the McArdle Histology Lab. Paraffin-embedded 5–10-μm sections were stained with hematoxylin and eosin, and pathological diagnoses were determined by two independent investigators. Color images were captured using a Pixera digital camera and processed using Adobe Photoshop.

Terminal deoxynucleotidyltransferase-mediated UTP end labeling (TUNEL) using TdT and dUTP-FITC TUNEL labeling was per the manufacturer's directions (Roche). Images were captured as described (Mirzoeva and Petrini 2001).

Meiotic spreads

Preparation, staining, and analyses of meiotic spreads from 1- to 4-mo-old testes using mouse Cor1 and human CREST antisera were as described (Dobson et al. 1994).

Hematopoietic cell preparations and analyses

Single-cell suspensions of lymphoid tissues were depleted of red blood cells by hypotonic lysis and maintained in PBS/3% FBS. Biotin- and fluorochrome-labeled antibodies specific for B220 (r-PE), CD43 (biotin), IgM (FITC), CD4 (r-PE), CD8 (FITC), and Streptavidin (FITC) were from Pharmingen. Dead cells were excluded by staining with 7-AAD (Molecular Probes) or propidium iodide. FACS analyses were performed on FACSCaliber instruments (Becton Dickinson).

Peripheral blood was collected in heparinized capillary tubes and transferred to EDTA-coated microtubes. Blood cell counts were done with an Advia 120 Hematology System (Bayer) at the University of Wisconsin Veterinary School Clinical Pathology Laboratory.

V(D)J recombination assays

Semiquantitative PCR and Southern blot analysis of immunoglobulin and TCRβ gene segment rearrangements were as described (Schlissel et al. 1991; Sikes et al. 1999). Thymus DNA from three 1-wk-old *Rad50*$^{+/+}$, *Rad50*$^{S/S}$, and *scid* mice was prepared and pooled for use in the ligation-mediated PCR assay as described (Zhu and Roth 1995). Transient recombination assays in transformed MEFs were as described (Errami et al. 1998) using *pMS127 (Rag1)* and *pMS216E (Rag2)* expression vectors. *JH290* rearrangements were amplified and sequenced as described (Taccioli et al. 1993).

Cell transfers

Four-week-old recipient mice were irradiated with 9–12 Gy from a Mark I ^{137}Cs source at 2.5 Gy/min, and retro-orbitally injected 2 h later with 5 million E16 fetal liver cells. FACS of hematopoietic tissues was done 4–6 wk posttransfer. DNA extracts (Schlissel et al. 1991) from reconstituting cells were genotyped by PCR.

Chromosome analyses

Metaphase cells prepared as described (van Steensel et al. 1998) were used for FISH as described (Lansdorp et al. 1996) using an FITC-conjugated peptide nucleic acid $(CCCTAA)_3$ probe or stained 15 min in 5% Giemsa (Sigma) for phase contrast analyses. For SKY analysis, metaphase cells were prepared using standard cytogenetic techniques (Roulston and Le Beau 1997) with the following modifications. Following mitotic arrest (2 h in 0.05μg/mL Colcemid, Invitrogen Life Technologies), cells were incubated 8 min in 0.075M KCl (37°C), and 2 mL fixative (3:1 absolute methanol:glacial acetic acid) was added dropwise. Cells were mixed, centrifuged, and resuspended in fresh fixative; the fixative step was repeated 3–6×, and air-dried slides were prepared. Differences in abundance of chromosome aberrations between genotypes were not correlated to culture duration.

Spectral karyotype (SKY) analysis

The SKY analysis was performed using the Applied Spectral Imaging (ASI) SkyPaint kit for mouse chromosomes. Slides were aged at room temperature for 1–14 days, pretreated for 15 min in 2×SSC (pH 7.0, 37°C), and washed 2× for 5 min each in PBS and 1× for 5 min in PBS/0.05M MgCl2. Slides were then incubated 10 min in 1% formaldehyde in PBS/0.05 M MgCl2, washed 5 min in PBS, and dehydrated in a graded ethanol series. Chromosomal DNA was denatured in 70% formamide/2×SSC (pH 7.0, 72°C, 2 min), and dehydrated in a graded ethanol series. The SKY probe mixture was denatured for 7 min at 75°C, incubated 1–2 h at 37°C, and then 10 μL of probe was applied to each slide. Slides were covered, sealed, and incubated 48 h (37°C). Unhybridized probe was removed by washing 3× for, 5 min each in 50% formamide/2×SSC (pH 7.0, 45°C,) and 2× for 5 min each in 1×SSC (45°C). Probe detection using SkyPaint; reagents was per the manufacturer's recommendations. Images were acquired using an SD-200 Spectracube (ASI) mounted on a Zeiss Axioplan 2. Analysis was performed using ASI image capturing (SI 2.2) and analysis software (SkyView 1.6). At least 10 metaphase cells were analyzed per lymphoma. Mouse chromosomes were classified according to the standardized karyotype refined by Cowell (1984).

Acknowledgments

We thank Santos Franco, Michelle Yao, Sheila Bitts, and Elizabeth M. Davis for technical contributions; Jennifer Salna, Mark Hughes, and Eric Michaels for animal care and management; Titia de Lange and the members of her lab for advice and reagents, especially Jan Karlseder and Agata Smogorzewska; Nadine Kolas, Peter Moens, and Nagendra Singh for providing invaluable technical instruction; members of the Petrini Lab, Wes Dunnick, and Andy Koff for critical comments on the manuscript; and William Morgan for help with chromosome analysis. C.F.B. was supported by an NSF Graduate Research Fellowship and a Wisconsin Alumni Research Foundation fellowship. R.S. was supported by NIH grant RR00144-01A1. L.E.H. was sup-

ported by an NIH predoctoral fellowship (T32-AI07495). M.M.L. was supported by NIH grant PHS U01 CA84221. D.B.R. is an Assistant Investigator of the Howard Hughes Medical Institute, and this work is supported in part by a grant from the NIH to D.B.R. (AI-36420). M.L.S. and E.O. are supported by NIH grants AI36944 and AI01412. J.H.J.P. is supported by an HFSPO grant and NIH grant GM56888. This is manuscript #3590 from the University of Wisconsin-Madison Laboratory of Genetics.

The publication costs of this article were defrayed in part by payment of page charges. This article must therefore be hereby marked "advertisement" in accordance with 18 USC section 1734 solely to indicate this fact.

References

Alani, E., Padmore, R., and Kleckner, N. 1990. Analysis of wild-type and *rad50* mutants of yeast suggests an intimate relationship between meiotic chromosome synapsis and recombination. *Cell* **61:** 419–436.

Baudat, F., Manova, K., Yuen, J.P., Jasin, M., and Keeney, S. 2000. Chromosome synapsis defects and sexually dimorphic meiotic progression in mice lacking Spo11. *Mol. Cell* **6:** 989–998.

Bressan, D.A., Olivares, H.A., Nelms, B.E., and Petrini, J.H.J. 1998. Alteration of N-terminal phosphoesterase signature motifs inactivates *Saccharomyces cerevisiae* Mre11. *Genetics* **150:** 592–600.

Bressan, D.A., Baxter, B.K., and Petrini, J.H.J. 1999. The Mre11/Rad50/Xrs2 protein complex facilitates homologous recombination-based double strand break repair in *Saccharomyces cerevisiae*. *Mol. Cell. Biol.* **19:** 7681–7687.

Carney, J.P., Maser, R.S., Olivares, H., Davis, E.M., Le Beau, M., Yates, J.R., 3rd, Hays, L., Morgan, W.F., and Petrini, J.H.J. 1998. The hMre11/hRad50 protein complex and Nijmegen breakage syndrome: Linkage of double-strand break repair to the cellular DNA damage response. *Cell* **93:** 477–486.

Connelly, J.C., Kirkham, L.A., and Leach, D.R. 1998. The SbcCD nuclease of Escherichia coli is a structural maintenance of chromosomes (SMC) family protein that cleaves hairpin DNA. *Proc. Natl. Acad. Sci.* **95:** 7969–7974.

Costanzo, V., Robertson, K., Bibikova, M., Kim, E., Grieco, D., Gottesman, M., Carroll, D., and Gautier, J. 2001. Responses to DNA damage in Xenopus: Mre11 protein complex prevents double-strand break accumulation during chromosomal DNA replication. *Mol. Cell* **8:** 137–147.

Cowell, J.K. 1984. A photographic representation of the variability in the G-banded structure of the chromosomes in the mouse karyotype. A guide to the identification of the individual chromosomes. *Chromosoma* **89:** 294–320.

D'Amours, D. and Jackson, S.P. 2001. The yeast Xrs2 complex functions in S phase checkpoint regulation. *Genes & Dev.* **15:** 2238–2249.

de Jager, M., van Noort, J., van Gent, D.C., Dekker, C., Kanaar, R., and Wyman, C. 2001. Human Rad50/Mre11 is a flexible complex that can tether DNA ends. *Mol. Cell* **8:** 1129–1135.

de Lange, T. and Petrini, J.H.J. 2000. A new connection at human telomeres: Association of the Mre11 complex with TRF2. *Cold Spring Harbor Symposium Quantitative Biology* **65:** 265–274.

Debrauwere, H., Loeillet, S., Lin, W., Lopes, J., and Nicolas, A. 2001. Links between replication and recombination in Saccharomyces cerevisiae: A hypersensitive requirement for homologous recombination in the absence of Rad27 activity. *Proc. Natl. Acad. Sci.* **98:** 8263–8269.

Dobson, M.J., Pearlman, R.E., Karaiskakis, A., Spyropoulos, B., and Moens, P.B. 1994. Synaptonemal complex proteins: Occurrence, epitope mapping and chromosome disjunction. *J. Cell Sci.* **107:** 2749–2760.

Dolganov, G.M., Maser, R.S., Novikov, A., Tosto, L., Chong, S., Bressan, D.A., and Petrini, J.H.J. 1996. Human Rad50 is physically associated with hMre11: Identification of a conserved multiprotein complex implicated in recombinational DNA repair. *Mol. Cell. Biol.* **16:** 4832–4841.

Errami, A., He, D.M., Friedl, A.A., Overkamp, W.J., Morolli, B., Hendrickson, E.A., Eckardt-Schupp, F., Oshimura, M., Lohman, P.H., Jackson, S.P., and Zdzienicka, M.Z. 1998. XR-C1, a new CHO cell mutant which is defective in DNA-PKcs, is impaired in both V(D)J coding and signal joint formation. *Nucleic Acids Res.* **26:** 3146–3153.

Fromm, M. and Berg, P. 1982. Deletion mapping of DNA regions required for SV40 early region promoter function *in vivo*. *J. Mol. Appl. Genet.* **1:** 457–481.

Furuse, M., Nagase, Y., Tsubouchi, H., Murakami-Murofushi, K., Shibata, T., and Ohta, K. 1998. Distinct roles of two separable in vitro activities of yeast mre11 in mitotic and meiotic recombination *EMBO J.* **17:** 6412–6425.

George, J.W., Stohr, B.A., Tomso, D.J., and Kreuzer, K.N. 2001. The tight linkage between DNA replication and double-strand break repair in bacteriophage T4. *Proc. Natl. Acad. Sci.* **98:** 8290–8297.

Grenon, M., Gilbert, C., and Lowndes, N.F. 2001. Checkpoint activation in response to double-strand breaks requires the Mre11/Rad50/Xrs2 complex. *Nat. Cell Biol.* **3:** 844–847.

Haber, J.E. 1998. The many interfaces of Mre11. *Cell* **95:** 583–586.

Harrington, J.J. and Lieber, M.R. 1994. The characterization of a mammalian DNA structure-specific endonuclease. *EMBO J.* **13:** 1235–1246.

Herrera, E., Samper, E., Martin-Caballero, J., Flores, J.M., Lee, H.W., and Blasco, M.A. 1999. Disease states associated with telomerase deficiency appear earlier in mice with short telomeres. *EMBO J.* **18:** 2950–2960.

Hopfner, K.P., Karcher, A., Craig, L., Woo, T.T., Carney, J.P., and Tainer, J.A. 2001. Structural biochemistry and interaction architecture of the DNA double- strand break repair Mre11 nuclease and Rad50-ATPase. *Cell* **105:** 473–485.

Hopfner, K.P., Craig, L., Moncalian, G., Zinkel, R.A., Usui, T., Owen, B.A.L., Karcher, A., Henderson, B., Bodmer, J., McMurray, C.T., Carney, J.P., Petrini, J.H.J., and Tainer, J.A. 2002. Rad50 Zinc-hook is a structure joining Mre11 complexes in DNA recombination and repair. *Nature* **I418:** 562–566.

Ivanov, E.L., Korolev, V.G., and Fabre, F. 1992. *XRS2*, a DNA repair gene of *Saccharomyces cerevisiae*, is needed for meiotic recombination. *Genetics* **132:** 651–664.

Jacks, T., Remington, L., Williams, B.O., Schmitt, E.M., Halachmi, S., Bronson, R.T., and Weinberg, R.A. 1994. Tumor spectrum analysis in p53-mutant mice. *Curr. Biol.* **4:** 1–7.

Keeney, S. and Kleckner, N. 1995. Covalent protein-DNA complexes at the 5′ strand termini of meiosis-specific double-strand breaks in yeast. *Proc. Natl. Acad. Sci.* **92:** 11274–11278.

Keeney, S., Giroux, C.N., and Kleckner, N. 1997. Meiosis-specific DNA double-strand breaks are catalyzed by Spo11, a member of a widely conserved protein family. *Cell* **88:** 375–384.

Lansdorp, P.M., Verwoerd, N.P., van de Rijke, F.M., Dragowska, V., Little, M.T., Dirks, R.W., Raap, A.K., and Tanke, H.J. 1996. Heterogeneity in telomere length of human chromosomes. *Hum. Mol. Genet.* **5:** 685–691.

Leach, D.R. 1994. Long DNA palindromes, cruciform struc-

tures, genetic instability and secondary structure repair. *Bioessays* **16:** 893–900.

Lee, H.W., Blasco, M.A., Gottlieb, G.J., Horner II, J.W., Greider, C.W., DePinho, R.A. 1998. Essential role of mouse telomerase in highly proliferative organs. *Nature* **392:** 569–574.

Lee, S.E., Bressan, D.A., Petrini, J.H., and Haber, J.E. 2002. Complementation between N-terminal *Saccharomyces cerevisiae* mre11 alleles in DNA repair and telomere length maintenance. *DNA Repair* **1:** 27–40.

Lim, D.S., Kim, S.T., Xu, B., Maser, R.S., Lin, J., Petrini, J.H.J., and Kastan, M.B. 2000. ATM phosphorylates p95/Nbs1 in an S-phase checkpoint pathway. *Nature* **404:** 613–617.

Lobachev, K.S., Gordenin, D.A., and Resnick, M.A. 2002. The Mre11 complex is required for repair of hairpin-capped double-strand breaks and prevention of chromosome rearrangements. *Cell* **108:** 183–193.

Lombard, D.B. and Guarente, L. 2000. Nijmegen breakage syndrome disease protein and MRE11 at PML nuclear bodies and meiotic telomeres. *Cancer Res.* **60:** 2331–2334.

Luo, G., Yao, M.S., Bender, C.F., Bladl, A.R., Bradley, A., and Petrini, J.H.J. 1999. Disruption of *mRad50* causes ES cell lethality, abnormal embryonic development and sensitivity to ionizing radiation. *Proc. Natl. Acad. Sci.* **96:** 7376–7381.

Ma, Y., Pannicke, U., Schwarz, K., and Lieber, M.R. 2002. Hairpin opening and overhang processing by an Artemis/DNA-dependent protein kinase complex in nonhomologous end joining and V(D)J recombination. *Cell* **108:** 781–794.

Maser, R.S., Monsen, K.J., Nelms, B.E., and Petrini, J.H.J. 1997. hMre11 and hRad50 nuclear foci are induced during the normal cellular response to DNA double strand breaks. *Mol. Cell. Biol.* **17:** 6087–6096.

Maser, R.S., Mirzoeva, O.K., Wells, J., Olivares, H., Williams, B.R., Zinkel, R.A., Farnham, P.J., and Petrini, J.H. 2001. Mre11 complex and DNA replication: Linkage to E2F and sites of DNA synthesis. *Mol. Cell Biol.* **21:** 6006–6016.

McBlane, J.F., van Gent, D.C., Ramsden, D.A., Romeo, C., Cuomo, C.A., Gellert, M., and Oettinger, M.A. 1995. Cleavage at a V(D)J recombination signal requires only RAG1 and RAG2 proteins and occurs in two steps. *Cell* **83:** 387–395.

Mirzoeva, O.K. and Petrini, J.H. 2001. DNA damage-dependent nuclear dynamics of the mre11 complex. *Mol. Cell Biol.* **21:** 281–288.

Moore, J.K. and Haber, J.E. 1996. Cell cycle and genetic requirements of two pathways of nonhomologous end-joining repair of double-strand breaks in *Saccharomyces cerevisiae*. *Mol. Cell. Biol.* **16:** 2164–2173.

Moreau, S., Furgeson, J.R., and Symington, L.S. 1999. The nuclease activity of Mre11 is required for meiosis but not for mating type switching, end joining, or telomere maintenance. *Mol. Cell Biol.* **19:** 556–566.

Mortensen, R.M., Zubiaur, M., Neer, E.J., and Seidman, J.G. 1991. Embryonic stem cells lacking a functional inhibitory G-protein subunit (alpha i2) produced by gene targeting of both alleles. *Proc. Natl. Acad. Sci.* **88:** 7036–7040.

Nagy, A., Moens, C., Ivanyi, E., Pawling, J., Gertsenstein, M., Hadjantonakis, A.K., Pirity, M., and Rossant, J. 1998. Dissecting the role of N-myc in development using a single targeting vector to generate a series of alleles. *Curr. Biol.* **8:** 661–664.

Nairz, K. and Klein, F. 1997. mre11S—a yeast mutation that blocks double-strand-break processing and permits nonhomologous synapsis in meiosis. *Genes & Dev.* **11:** 2272–2290.

Nelms, B.E., Maser, R.S., MacKay, J.F., Lagally, M.G., and Petrini, J.H.J. 1998. In situ visualization of DNA double-strand break repair in human fibroblasts. *Science* **280:** 590–592.

Paull, T.T. and Gellert, M. 1998. The 3′ to 5′ exonuclease activity of Mre 11 facilitates repair of DNA double-strand breaks. *Mol. Cell* **1:** 969–979.

———. 1999. Nbs1 potentiates ATP-driven DNA unwinding and endonuclease cleavage by the Mre11/Rad50 complex. *Genes & Dev.* **13:** 1276–188.

Paull, T.T., Rogakou, E.P., Yamazaki, V., Kirchgessner, C.U., Gellert, M., and Bonner, W.M. 2000. A critical role for histone H2AX in recruitment of repair factors to nuclear foci after DNA damage. *Curr. Biol.* **10:** 886–895.

Petrini, J.H. 2000a. The Mre11 complex and ATM: Collaborating to navigate S phase. *Curr. Opin. Cell Biol.* **12:** 293–296.

Petrini, J.H.J. 2000b. S phase functions of the Mre11 complex. *Cold Spring Harb. Symp. Quant. Biol.* **65:** 405–412.

Prives, C. and Hall, P.A. 1999. The p53 pathway. *J. Pathol.* **187:** 112–126.

Rogakou, E.P., Boon, C., Redon, C., and Bonner, W.M. 1999. Megabase chromatin domains involved in DNA double-strand breaks in vivo. *J. Cell Biol.* **146:** 905–916.

Romanienko, P.J. and Camerini-Otero, R.D. 2000. The mouse *Spo11* gene is required for meiotic chromosome synapsis. *Mol. Cell* **6:** 975–987.

Roth, D.B., Menetski, J.P., Nakajima, P.B., Bosma, M.J., and Gellert, M. 1992. V(D)J recombination: Broken DNA molecules with covalently sealed (hairpin) coding ends in scid mouse thymocytes. *Cell* **70:** 983–991.

Roulston, D. and Le Beau, M.M. 1997. Cytogenetic analysis of hematologic malignant disease. In *The AGT cytogenetics laboratory manual* (eds. M.J. Barch, T. Knutsen, and J. Spurbeck), pp. 325–374. Lippincott-Raven, Philadelphia, PA.

Rudolph, K.L., Chang, S., Lee, H.W., Blasco, M., Gottlieb, G.J., Greider, C., and DePinho, R.A. 1999. Longevity, stress response, and cancer in aging telomerase-deficient mice. *Cell* **96:** 701–712.

Schlissel, M.S., Corcoran, L.M., and Baltimore, D. 1991. Virus-transformed pre-B cells show ordered activation but not inactivation of immunoglobulin gene rearrangement and transcription. *J. Exp. Med.* **173:** 711–720.

Sikes, M.L., Suarez, C.C., and Oltz, E.M. 1999. Regulation of V(D)J recombination by transcriptional promoters. *Mol. Cell Biol.* **19:** 2773–2781.

Stewart, G., Maser, R.S., Stankovic, T., Bressan, D.A., Kaplan, M.I., Jaspers, N.G.J., Byrd, P.J., Petrini, J.H.J., and Taylor, A.M.R. 1999. The DNA double strand break repair gene hMre11, is mutated in individuals with a new ataxia telangiectasia like disorder (ATLD). *Cell* **99:** 577–587.

Stohr, B.A. and Kreuzer, K.N. 2001. Repair of topoisomerase-mediated DNA damage in bacteriophage T4. *Genetics* **158:** 19–28.

Symington, L.S. 1998. Homologous recombination is required for the viability of rad27 mutants. *Nucleic Acids Res.* **26:** 5589–5595.

Taccioli, G.E., Rathbun, G., Oltz, E., Stamato, T., Jeggo, P.A., and Alt, F.W. 1993. Impairment of V(D)J recombination in double-strand break repair mutants. *Science* **260:** 207–210.

Tsubouchi, H. and Ogawa, H. 1998. A novel *mre11* mutation impairs processing of double-strand breaks of DNA during both mitosis and meiosis. *Mol. Cell. Biol.* **18:** 260–268.

Usui, T., Ohta, T., Oshiumi, H., Tomizawa, J., Ogawa, H., and Ogawa, T. 1998. Complex formation and functional versatility of Mre11 of budding yeast in recombination. *Cell* **95:** 705–716.

Usui, T., Ogawa, H., and Petrini, J.H. 2001. A DNA damage response pathway controlled by Tel1 and the Mre11 complex. *Mol. Cell* **7:** 1255–1266.

van Steensel, B., Smogorzewska, A., and de Lange, T. 1998. TRF2 protects human telomeres from end-to-end fusions.

Cell **92:** 401–413.
Ward, I.M. and Chen, J. 2001. Histone H2AX is phosphorylated in an ATR-dependent manner in response to replicational stress. *J. Biol. Chem.* **276:** 47759–47762.
Weissman, I.L. 2000. Stem cells: Units of development, units of regeneration, and units in evolution. *Cell* **100:** 157–168.
Williams, B.R., Mirzoeva, O.K., Morgan, W.F., Lin, J., Dunnick, W., and Petrini, J.H. 2002. A murine model of nijmegen breakage syndrome. *Curr. Biol.* **12:** 648–653.
Xiao, Y. and Weaver, D.T. 1997. Conditional gene targeted deletion by Cre recombinase demonstrates the requirement for the double-strand break repair Mre11 protein in murine embryonic stem cells. *Nucleic Acids Res.* **25:** 2985–2991.
Yamaguchi-Iwai, Y., Sonoda, E., Sasaki, M.S., Morrison, C., Haraguchi, T., Hiraoka, Y., Yamashita, Y.M., Yagi, T., Takata, M., Price, et al. 1999. Mre11 is essential for the maintenance of chromosomal DNA in vertebrate cells. *EMBO J.* **18:** 6619–6629.
Zhu, C. and Roth, D.B. 1995. Characterization of coding ends in thymocytes of scid mice: Implications for the mechanism of V(D)J recombination. *Immunity* **2:** 101–112.
Zhu, X.-D., Kuster, B., Mann, M., Petrini, J.H.J., and de Lange, T. 2000. Cell cycle regulated association of Rad50/Mre11/Nbs1 with TRF2 and human telomeres. *Nat. Genet.* **25:** 347–352.
Zhu, J., Petersen, S., Tessarollo, L., and Nussenzweig, A. 2001. Targeted disruption of the Nijmegen breakage syndrome gene NBS1 leads to early embryonic lethality in mice. *Curr. Biol.* **11:** 105–109.